COBEM 2023 27TH INTERNATIONAL CONGRESS OF MECHANICAL ENGENEERING

ABCM Brazilian Society of Mechanical Sciences and Engineering
27th ABCM International Congress of Mechanical Engineering
December 04-08, 2023, Florianópolis-SC, Brazil

COB-2023-0469
HETEROGENEOUS REACTING SYSTEM EVALUATION BY CFD MODEL OF SEMI INDUSTRIAL SCALE GASIFIER IN FLUIDIZED-BED

Vitor Alberto Lemes Monteiro
Marcelo Braga dos Santos
Department of Mechanical Engineering, Federal University of Uberlândia, Av. João Naves de Ávila, 2121, 38408-100
vitoralbertolemes@hotmail.com, marcelo.bragadossantos@ufu.br

Alam Gustavo Trovó
Chemistry Institute, Federal University of Uberlândia, Av. João Naves de Ávila, 2121, 38408-100, Uberlândia-MG
alamtrovo@ufu.br

Solidônio Rodrigues de Carvalho
Department of Mechanical Engineering, Federal University of Uberlândia, Av. João Naves de Ávila, 2121, 38408-100
solidonio@ufu.br

Abstract. *Gasification in fluidized-bed reactors is a crucial topic that pertains to Waste to Energy systems. However, there are no readily available solutions for efficient and reliable simulations that can be used to design or control such units. The aim of this study is to develop a model that can be used to evaluate some of the heterogeneous reactions that occur during the gasification of biomass in a semi-industrial scale reactor. These reactions are a part of the thermal degradation of biomass and are unique due to the conversion of its phase from solid to gas. The study utilized the Eulerian-Eulerian approach, which involved using OpenFOAM software to create a computational fluid dynamic system to simulate selected reactions. The model involved a bubbling fluidized-bed reactor that contained silica sand as a bed material, and a specific gas injection (CO_2, H_2O, and H_2 depending on reaction simulated) was used for the simulation of gasification subprocesses of a generic carbonaceous biomass. The results showed a quantitative and consistent progression of the thermal degradation process in terms of the solid-phase transformations of biomass into gas for each chemical reaction. Additionally, the Reacting Zone was identified and analyzed more effectively. This detailed evaluation of such reactions is essential for the author's research line studies, which includes the development of a large-scale gasifier of municipal refuse-derived fuel in a fluidized bed.*

Keywords: *Eulerian-Eulerian approach, Large-Scale, Gasification, Multiphase flow, Phase change*

1. INTRODUCTION

Our research group focuses on WTE (Waste to Energy) technologies, specifically studying a semi-industrial scale fluidized bed gasification plant to convert municipal solid waste (MSW) into energy. Previous studies have demonstrated the production of municipal refuse-derived fuel (MRDF) biomass from MSW using a solid waste processing line (SWPL) (Infiesta et al., 2019; Ferreira et al., 2021). Our research group has also developed an experimental fluidized bed gasification reactor capable of recovering syngas from MRDF. The goal for the future is to create a comprehensive Computational Fluid-Dynamics (CFD) model that can simulate the reactor process and improve this gasification technology for WTE.
The objective of this paper is to incorporate heterogeneous reactions into the computational model, specifically evaluating the conversion of solid particles into the gaseous phase.

2. MATERIALS AND METHODS

The gasification process was represented by some sub-processes (Figure 1) involving the devolatilization, drying, homogeneous and heterogeneous reactions. The final product of the reactor is the conversion of the solid biomass in a combustible gas, named syngas. The development of the mentioned semi-industrial scale gasifier model consists of 9.975 m height and 1.46 m of diameter (Figure 2). Such reactor have been studied even in terms of its fluidization phenomena with CFD large-scale simulations (Monteiro et al., 2023).

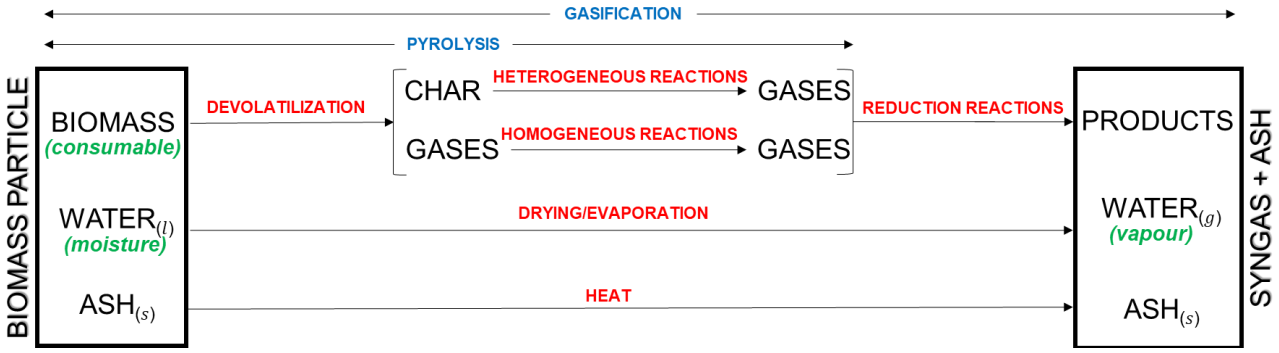

Figure 1. Biomass gasification modeling steps

In this study, the geometry of the reactor was simplified, and its specific details (such as the cyclone) were omitted to focus on evaluating the heterogeneous reactions of biomass (as shown in Figure 2d). This approach allows for better control over the reactions, which in turn provides clearer and more accurate results for the evaluation of each individual reaction.

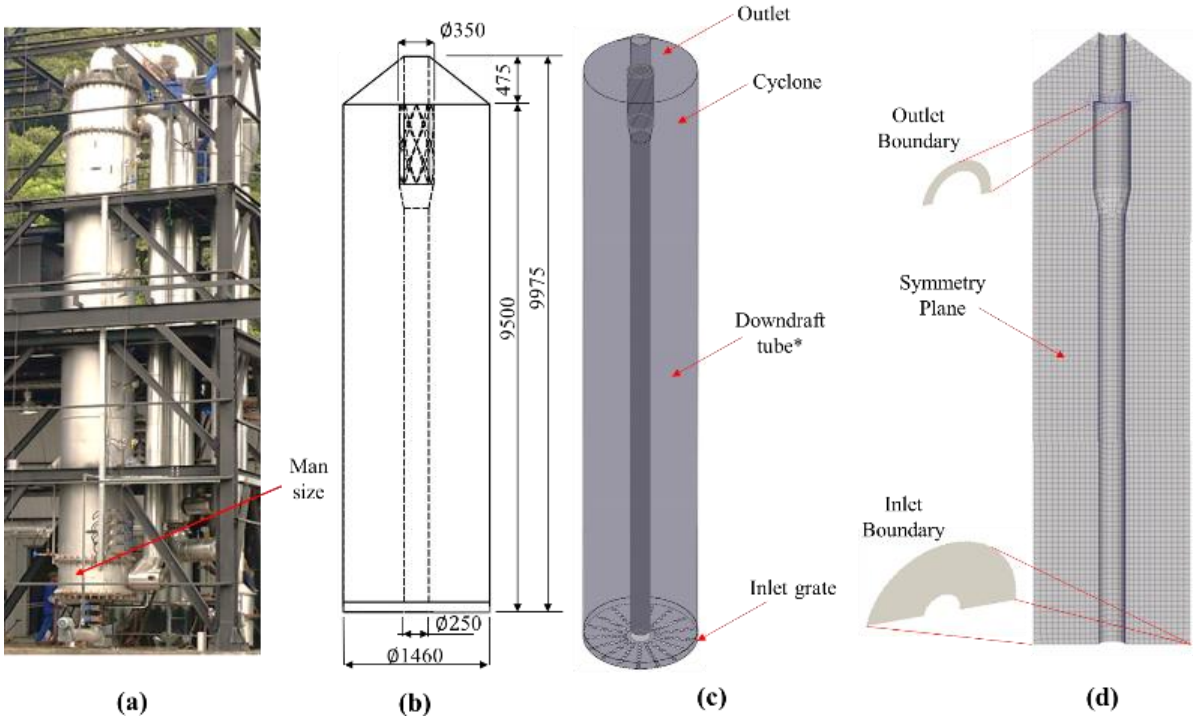

Figure 2. (a) Semi-industrial reactor, showing the real dimensions, compared with the size of a man. (b) Reactor geometry (dimensions in mm). (c) 3D design of the gasifier. (d) Mesh layout and main boundaries. *Downdraft tube for extraction of particles (ash and silica sand) at the bottom of the reactor

The CFD system used in this study is comprised of three components: the gas phase, biomass particles, and silica sand - the latter two being solid phases. The biomass particles phase was treated as a full carbon particle ($C_{(s)}$), while the gas phase included all the gaseous species, such as H_2O, CO_2, CO, H_2, O_2, N_2 and CH_4; some species were suppressed in graphic results. The heterogeneous reactions that were analyzed in this study involve the reaction of a gaseous species with the solid carbon, producing only gaseous species. As such, for each reaction simulation, the inlet gas was composed of 100% of the reagent gas for that specific reaction (i.e. CO_2, H_2O or H_2).

2.1 Governing Equations

The Eulerian-Eulerian approach employed in this study solves the governing equations for each phase individually, ensuring that the sum of the volumetric particle fraction of all phases always equals unity. The governing equations for

each phase were implemented using a computational methodology outlined by *Rusche* (2002), which is briefly summarized below.

The mass balance equation is expressed as:

$$\frac{\partial}{\partial t}\alpha_k\rho_k + \frac{\partial}{\partial x_i}\alpha_k\rho_k U_k = \dot{m}_k + \dot{m}_{p\to k} \tag{1}$$

The momentum equations are,

$$\frac{\partial}{\partial t}(\alpha_k\rho_k U_k) + \nabla\cdot(\alpha_k\rho_k U_k U_k) = \alpha_k\rho_k g_i + \nabla\cdot S_k + I_k \tag{2}$$

$$S_k = \nabla\cdot(\alpha_k\tau_k) - \alpha_k\nabla p - \nabla p_k \tag{3}$$

$$\tau_k = \mu_{eff}\frac{1}{2}\left[\nabla U_k + \nabla U_k^T\right] + \left(\lambda_k - \frac{2}{3}\mu_{eff}\right)(\nabla\cdot U_k)I \tag{4}$$

Energy balance equation is given as,

$$\frac{\partial}{\partial t}(\alpha_k\rho_k E_k) + \nabla\cdot(\alpha_k\rho_k U_k E_k) = \alpha_k\left(\frac{\partial p}{\partial t} + U_k\cdot\nabla p\right) - \nabla\left(\alpha_k\kappa_{eff}\nabla T_k\right) + \phi + A_{sp}h(T^* - T_k) + \dot{q}_k \tag{5}$$

The subscript k denotes either the solid or fluid phase, with α_k representing the volume fraction of the phase. For instance, α_p denotes the fraction of particles in the solid phase, while α_g denotes the fraction of gas in the continuous phase. The subscript i indicates each species present in either phase, with ρ_k and U_k representing the density and velocity of the respective phase. The mass source term is denoted by $\dot{m}_k$ while $\dot{m}_{p\to i,k}$ denotes the interphase mass transfer term from converted biomass particle products to the gas phase. The momentum equation describes S_k as the stress tensor or the respective phase, with ρ representing pressure and ρ_k representing the granular pressure for the solid phase. λ_k denotes the solid bulk viscosity, while I_k is the momentum exchange term, which includes drag forces and turbulent dispersion. k_{eff} and μ_{eff} represent the effective thermal conductivity and viscosity, which account for turbulent effects. In the energy transport equation, ϕ is the viscous dissipation, E_k is the enthalpy, A_{sp} is the superficial area per unit volume of the particle phase, h is the convective coefficient, and T^* is the temperature of the exchange phase. The heat source term for the k phase is denoted by $\dot{q}_k$. The drag model is a combination of the *Ergun* Equation (1952) and *Wen* and *Yu* drag model (Wen et al., 1966), with the drag factor being one for a spherical particle based on Schiller & Naumann (1935). This combination leads to *Gidaspow's* Drag Model (Gidaspow, 1994), which is recommended for dense particulate flow in this type of reactor. Empirical correlation is used to calculate the *Nusselt's* number for heat flux between phases.

$$Nu = 2 + 0.6Re^{0.5}\mathrm{Pr}^{0.33} \tag{6}$$

$$Nu = \frac{hd_p}{\kappa} \tag{7}$$

Using Eq. (6), the convective coefficient (h) for the energy transport equation (Eq. 5) is estimated. The *Sutherlands's* transport model (Sutherland, 1893) evaluates dynamic viscosity (μ) as function of temperature (T) of a specific coefficient (A_s) and of the Sutherland Temperature (T_s) as follow:

$$\mu = \frac{A_s\sqrt{T}}{1+\frac{T_s}{T}} \tag{8}$$

JANAF Thermochemical Tables (Chase, 1998) provides the coefficients of a polynomial relation to calculate the specific heat (c_p) as function of temperature (T).

The balance of mass fraction species (Y) is written as:

$$\frac{\partial}{\partial t}\left(\alpha_k\rho_k Y_{i,k}\right) + \nabla\cdot\left(\alpha_k\rho_k U_k Y_{i,k}\right) = \nabla\left(\alpha_k\rho_k \mathrm{D}_{\mathrm{eff}}\nabla Y_{i,k}\right) + \dot{m}_{p\to i,k} \tag{9}$$

As depicted in Figure 1, the software incorporates several reactions as part of the gasification process's heterogeneous balanced reactions. These reactions are as follows:

$$C_{(s)} + CO_{2(g)} \to 2CO_{(g)} \qquad \Delta H = 172\ kJ/mole \tag{10}$$

$$C_{(s)} + H_2O_{(g)} \rightarrow CO_{(g)} + H_{2(g)} \qquad \Delta H = 131\ kJ/mole \tag{11}$$

$$C_{(s)} + 2H_{2(g)} \rightarrow CH_{4(g)} \qquad \Delta H = -75\ kJ/mole \tag{12}$$

Equation (10) represents the Boudouard reaction, Equation (11) represents the reforming of char, and Equation (12) represents the methanation reaction, sometimes referred to as the hydrogasification reaction by certain authors. The thermal energy (ΔH) requirements described in (Hasse et al., 2021) have been incorporated into each reaction as a source term ($\dot{q}_k$) in the energy balance equation (Eq. 5).

The char consumption rate by each heterogeneous reaction (R_{het}) is determined by:

$$R_{het} = \frac{R_{kin}R_{diff}}{R_{kin}+R_{diff}}P_i \tag{13}$$

where R_{diff} and R_{kin} represent the diffusion rate and kinetic rate, respectively, and P_i is the partial pressure of the species (H_2O, CO_2 or H_2). These rates are expressed by the following equations (14) and (15):

$$R_{kin} = -AT^{\beta}\left(-\frac{E_a}{RT_p}\right) \tag{14}$$

where E_a denotes the activation energy, A is the frequency factor, β is the temperature exponent (set to unity in this case) – demonstrating linear dependence of rate on temperature –, T_p represents the particle temperature, and R is the gas constant.

$$R_{diff} = \frac{C_i\left[\frac{T_p+T_g}{2}\right]^{0.75}}{d_p} \tag{15}$$

Here, C_i refers to the mass diffusion rate constant, T_p and T_g correspond to the particle and gas temperatures, respectively, and d_p represents the particle diameter, which is calculated using the formula:

$$d_p = \left(\frac{6m_p}{\pi\rho_p}\right)^{\frac{1}{3}} \tag{16}$$

The parameters in Equation (14) and (15) are experimentally determined for each chemical reaction (Table 1).

Table 1. Rate constants for the heterogeneous reactions (Klimanek et al., 2018).

Reaction	A **[s/m]**	E_a **[J/kmol]**	C **[sK$^{-0.75}$]**
Boudouard	2.0×10^{-7}	7.9×10^{7}	5×10^{-12}
Reforming of Char	2.0×10^{-7}	7.9×10^{7}	5×10^{-12}
Methanation	1.18×10^{-5}	1.49×10^{8}	5×10^{-12}

$\dot{m}_{p\rightarrow i,k}$ are expressed in relation to the coefficients (n_i) of each element involved in the respective reactions (Eq. 10, 11, and 12):

$$\dot{m}_{p\rightarrow i,k} = n_i\left(\alpha_p\rho_pY_{char}\right)R_{het} \tag{17}$$

Here, R_{het} is specific to each reaction (Boudouard, reforming of char, or methanation), while Y_{char} represents the volumetric fraction of char derived from biomass particles.

Within this model, the shrinkage of particle diameter has not been considered, meaning that this parameter remains constant over time. Nonetheless, the consumption of biomass is implemented numerically by reducing the mass fraction of biomass particles through the consumption rate.

2.2 Multiphase system modeling

To simulate multi-phase systems, OpenFOAM uses the "interface composition phase change" approach (Ranz, W. E. and Marshall, 1952), which is based on modeling the interfaces between the phases and the phase changes that can occur

at these interfaces. This approach is particularly useful for simulating complex problems such as bubble formation, droplet breakup, and heat transfer between phases. Some models used were breathily described below from OpenFOAM User Guide (Greenshields, 2020).

The *interfaceCompositionPhaseChangeMultiphaseSystem* is a multi-phase model used by OpenFOAM to simulate multi-phase systems. This model is based on a set of equations that describe the dynamics of the interfaces between the phases and the phase changes that can occur at these interfaces. These equations are numerically solved by the software to obtain a solution for the multi-phase problem.

The present study employed a Computational Fluid Dynamics (CFD) model using the open-source software OpenFOAM, with the configuration options of Gidaspow viscosity and conductivity models, *Lun* granular pressure model, *Johnson-Jackson-Schaeffer* frictional stress model, and *Sinclair-Jackson* radial model. These models are commonly used for simulating gas-solid flows, particularly in the dense regime, and provide a robust and reliable tool for investigating the complex behavior of such flows.

2.3 Simulation Setup: Configuration of Bubbling Fluidized Bed Reactor

As previously mentioned, the gaseous phase in the reactor comprises H_2O, CO_2, CO, H_2, O_2, N_2 and CH_4, while the biomass phase consists of carbon. The reactor geometry, illustrated in Figure 2d, features the frontal face acting as a symmetry plane, reducing computational expenses. The mesh employed consists mainly of hexahedral cells, with some prism cells added to account for minor edge adjustments. All mesh regions possess an equal degree of refinement, and the geometry and mesh were constructed with OpenFOAM's *snappyHexMesh* utility. Four refinement levels were tested: coarse (8,434 cells), medium (26,972 cells), fine (61,744 cells), and finest (120,888 cells). However, due to computational expense and accuracy requirements, the fine mesh with 61,744 cells was utilized for modeling the reacting system phenomena. Initially, the reactor was filled with sand and biomass particles up to one-third of its height, which was subsequently infused with a continuous stream of gas. The total mass of the biomass particle was 71.32 kg (100% carbonaceous matter) and the sand weighed 2,641.54 kg. Table 2 displays some other simulation parameters. A constant time step of 1×10-3 was implemented, and a total integration time of 10 s was utilized to observe significant thermal degradation of the initial char mass and production of gaseous components. Additionally, less than 10 s was sufficient for stabilizing the bubbling in the fluidized bed reactor when the syngas composition and inlet pressure remained constant.

Table 2. Initial conditions and other parameters.

Parameters	Value
Biomass feed rate [kg/h]	N/A
Biomass temperature [K]	670
Biomass Particle diameter [m]	0.015
Biomass initial mass [kg]	71.32
Density of biomass (char) [kg/m³]	470
Energy source term [kg.m²/s³]	Eq. (10), (11) and (12)
Density of sand particles [kg/m³]	2500
Sand particles diameter [m]	0.003
Initial bed temperature [K]	1,093
Operating temperature [K]	1,093
Gasifier walls condition	Insulated
Interstitial inlet velocity [m/s]	1.5
Outlet pressure [kPa]	Atmospheric
Atmospheric pressure [kPa]	100

N/A – not applied

3. RESULTS AND DISCUSSION

Figure 3 illustrates the final state of the reactor after the simulation period, where the biomass particles fully composed of char remain evenly distributed at the top of the fluidized bed. Due to the diameter and specific mass of the char particles, they are not uniformly mixed with the sand particles at the bottom of the bed. This feature substantially affects the gas-forming and where the chemical reactions occur predominantly. The concentration of the char particles in this region characterizes the main Reacting Zone (RZ) of the thermochemical reactor. This region is characterized by the highest occurrence of the reaction(s) involved in the reactor, concentration of reactant biomass and formation of gaseous products. In a real reactor, it is a region that is not physically evident, internal to the reactor, but its identification can provide important information about the reactor's functionality. The heat generated from exothermic reactions is transferred to the gas and released outside of the reactor, which can affect the heat transfer of the char particles. Although ideally, the char

particles should be homogeneously mixed with sand during continuous operation, the generation of thermal energy at this zone may improve endothermic chemical reactions such as Methanation (Eq. 12).

As predicted by reactions from Eqs. (10), (11), and (12) depicted in Figure 5, Figure 6 and Figure 7, respectively, all produced species of the syngas increase with simulation time, while the insufflated species decrease. For example, during the Reforming of char reaction (Figure 6), there is the production of CO and H_2 species, which results in a decrease of H_2O within the reactor. Although the inlet insufflation of H_2O is constant, its chemical conversion causes the amount of this component to vary in the reactor, before it starts to stabilize. Similar patterns were observed in other reactions.

Under the given reactor configurations and fixed parameters (Table 2), the char particles were consumed and converted from solid to gaseous phase at a constant rate (Figure 4) since the temperature of the reactor and chemical rates remained constant. This qualitative observation was also noted in other reactions.

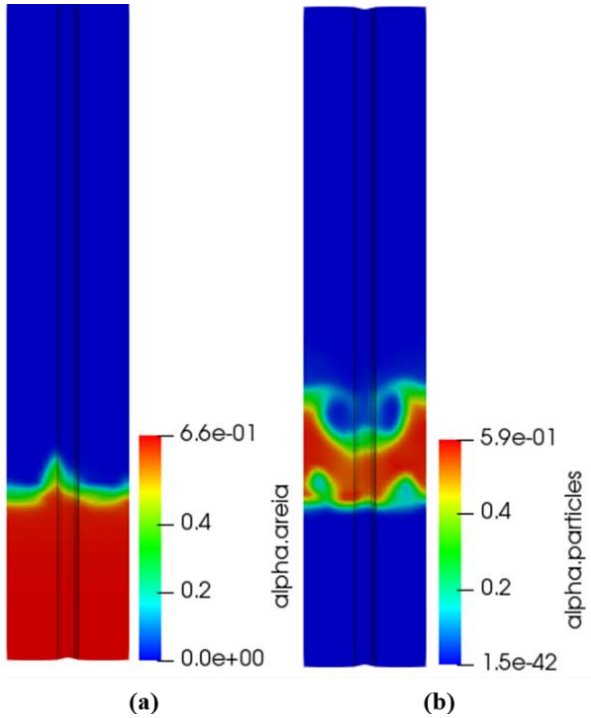

Figure 3. The overall characteristics of the reactor's internal fluid dynamics in any reaction simulation can be summarized in terms of (a) the mass fraction of particles and (b) the mass fraction of sand at the final stage of the simulations.

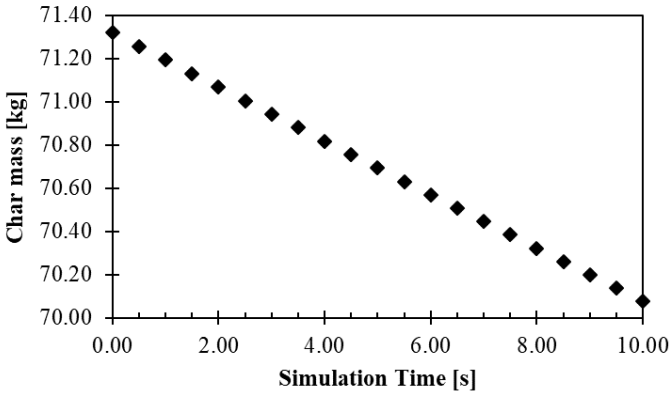

Figure 4. The consumption of char at a constant rate in the simulation of the Boudouard reaction.

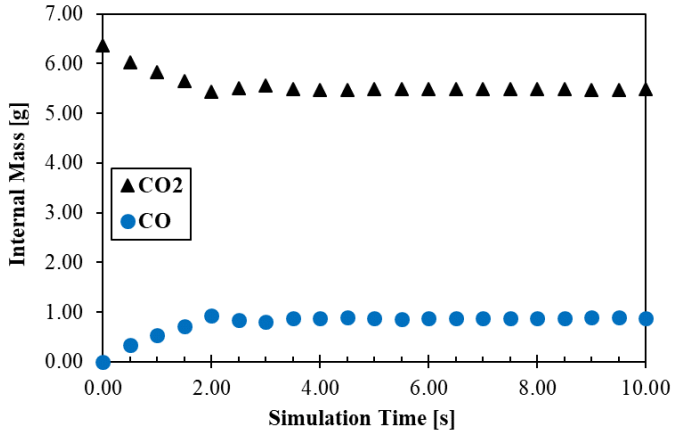

Figure 5. The gaseous species composition during the simulation of the Boudouard reaction.

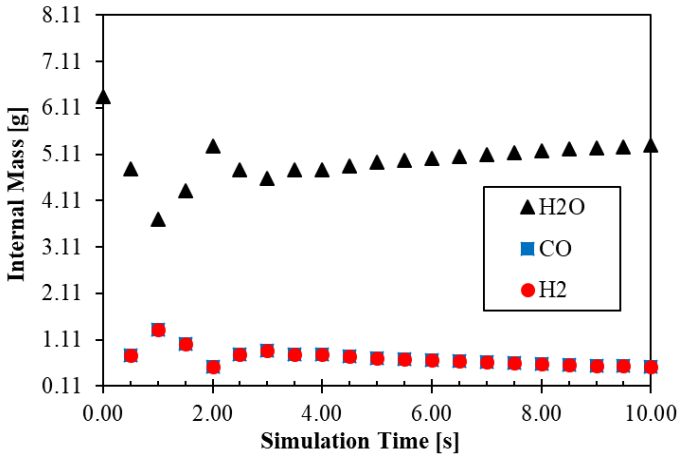

Figure 6. Composition of the gaseous species during simulation of Reforming of char reaction

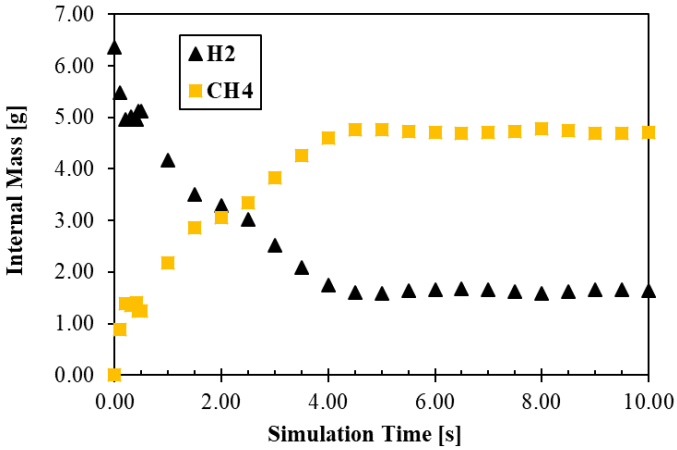

Figure 7. Composition of the gaseous species during simulation of Methanation reaction

All gaseous species produced and consumed in each reaction are displayed separately in Figure 8, Figure 9 and Figure 10 at the final time step of the simulation. As mentioned, the highest concentration of produced gases is near the char particles, which surround the reaction zone (RZ). The reactant species (CO_2, H_2O, or H_2) injected into the bottom of the reactor are homogeneous until they reach the RZ, where they are diluted into the other produced components.

After 5 seconds of simulation time, the system reaches a steady state where the bubbling fluid dynamics show no significant changes, and the inlet pressure remains stable (Figure 3). However, the chemical reactions do not follow the same pattern and require approximately 3 seconds (Figure 5), 10 seconds (Figure 6), and 5 seconds (Figure 7) to obtain a constant composition of syngas for the Boudouard, Reforming of Char, and Methanation reactions, respectively. Other

simulations performed at lower inlet velocities, in a smooth fluidized bed, take more time to reach a chemical steady state. This indicates that the fluid dynamics of the reactor significantly affect the chemistry. Therefore, in this bubbling fluidized bed reactor, the reactions reach a continuous regime in less time than in a smooth fluidized bed reactor. This feature supports the phase transfer of heterogeneous and devolatilization reactions, which is significantly different from a fixed bed reactors, for example, making fluidized bed reactors suitable for semi-industrial biomass gasification. This information will be considered in future works, as it is important to determine the minimum time required to achieve a continuous operating condition in a semi-industrial scale gasifier.

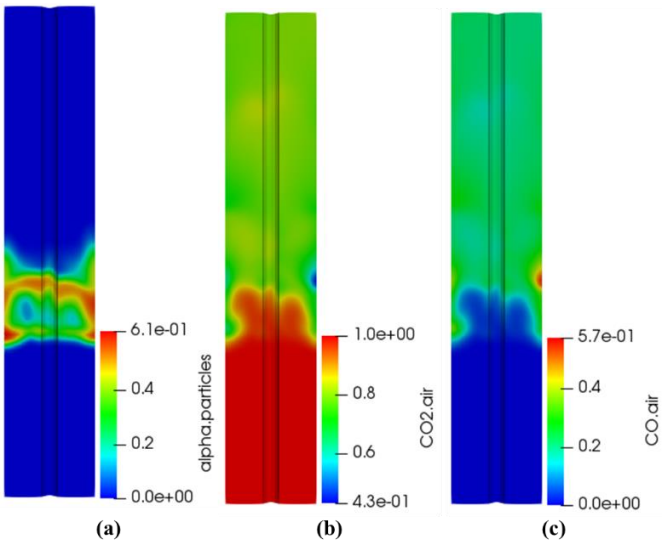

Figure 8. (a) The arrangement of biomass particles and the resulting composition of the reactor in the simulation of the Boudouard reaction, specifically focusing on (b) CO_2 and (c) CO.

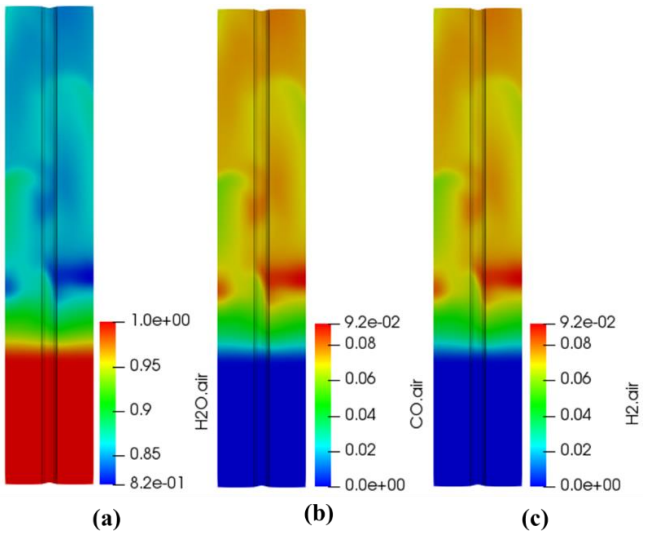

Figure 9. Final composition of the reactor at Reforming of char reaction simulation. (a) H_2O, (b) CO and (c) H_2

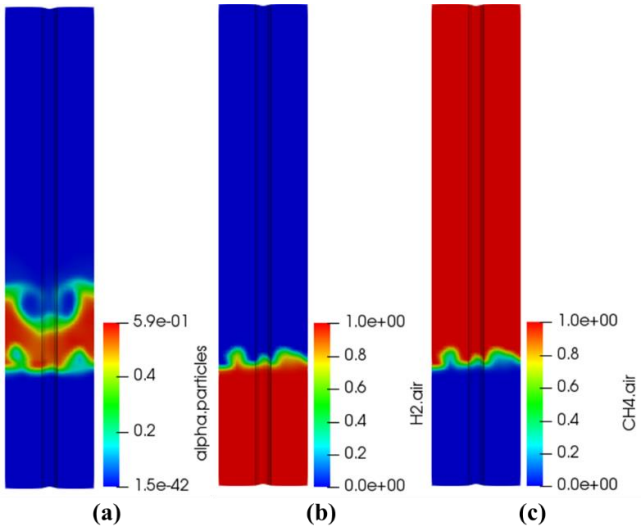

Figure 10. (a) Disposition of (biomass) particles and final composition of the reactor at Methanation reaction simulation. (a) H_2 and (b) CH_4

4. CONCLUSION

The aim of this study was to evaluate the implementation of chemical heterogeneous reactions using computational fluid dynamics (CFD), including the main heterogeneous phenomena of phase transfer, present in many reactions involved in gasification processes. The implementation of any heterogeneous reactions, including combustion reactions, within the Eulerian-Eulerian approach was found to be feasible.

The simulations provided valuable information regarding *(i)* the functionality of the thermochemical reactor, *(ii)* identification of the main reacting zone and *(iii)* the time required for fluid-dynamic and chemical stabilization. The implementation of chemical reactions produced consistent results, representing the consumption of char particles, reaction with the gaseous agent, and production of other species. The mass transfer between phases was also satisfactory, and the energy source term of each chemical reaction was well-arranged within the fluid-dynamic system.

This implementation is part of a larger effort to develop a fully CFD model to represent a semi-industrial scale gasifier as part of the authors' research program.

5. ACKNOWLEDGEMENTS

The authors are grateful for the financial support provided by Furnas Centrais Elétricas S.A., Carbogás Energia Ltda., Agência Nacional de Energia Elétrica, Coordenação de Aperfeiçoamento de Pessoal de Nível Superior (CAPES), Conselho Nacional de Desenvolvimento Científico e Tecnológico (CNPq), and Fundação de Amparo à Pesquisa do Estado de Minas Gerais (FAPEMIG) and Financiadora de Estudos e Projetos (FINEP).

Vitor A. L. Monteiro is grateful to Empresa Brasileira de Serviços Hospitalares (EBSERH).

6. REFERENCES

Chase, M. W., NIST-JANAF Thermochemical Tables, 4th Ed. J. Phys. Chem. Ref. Data. 1998, Monograph 9(Part I and Part II), *Journal of Physical and Chemical Reference Data*, 1998.

Ergun, S., Fluid Flow through Packed Columns, 1952.

Ferreira, C. R. N., Infiesta, L. R., Monteiro, V. A. L., Starling, M. C. V. M., Silva Júnior, W. M. da, Borges, V. L., Carvalho, S. R. and Trovó, A. G., Gasification of Municipal Refuse-Derived Fuel as an Alternative to Waste Disposal: Process Efficiency and Thermochemical Analysis, *Process Safety and Environmental Protection*, vol. **149**, no. x, pp. 885–93, 2021. DOI: 10.1016/j.psep.2021.03.041

Gidaspow, D., *Multiphase Flow and Fluidization: Continuum and Kinetic Theory Descriptions*, *Multiphase Flow and Fluidization: Continuum and Kinetic Theory Descriptions*, pp. 1–467, 1994.

Greenshields, C. J., OpenFOAM, no. July, 2020.

Hasse, C., Debiagi, P., Wen, X., Hildebrandt, K., Vascellari, M. and Faravelli, T., Advanced Modeling Approaches for CFD Simulations of Coal Combustion and Gasification, *Progress in Energy and Combustion Science*, vol. **86**, no. September 2020, p. 100938, from https://doi.org/10.1016/j.pecs.2021.100938, 2021. DOI: 10.1016/j.pecs.2021.100938

Infiesta, L. R., Ferreira, C. R. N., Trovó, A. G., Borges, V. L. and Carvalho, S. R., Design of an Industrial Solid Waste

Processing Line to Produce Refuse-Derived Fuel, *Journal of Environmental Management*, vol. **236**, no. August 2018, pp. 715–19, from https://doi.org/10.1016/j.jenvman.2019.02.017, 2019. DOI: 10.1016/j.jenvman.2019.02.017

Klimanek, A. and Bigda, J., CFD Modelling of CO2 Enhanced Gasification of Coal in a Pressurized Circulating Fluidized Bed Reactor, *Energy*, vol. **160**, pp. 710–19, 2018. DOI: 10.1016/j.energy.2018.07.046

Monteiro, V. A. L., Reis, M. G. A., Infiesta, L. R., Ferreira, C. R. N., Santos, M. B. dos, Trovó, A. G. and Carvalho, S. R., Eulerian Computational Fluidisation Modelling Using OpenFOAM Applied to a Semi-Industrial Fluidised Bed Reactor and Pilot Plant Application, *Cleaner Chemical Engineering*, vol. **5**, no. December 2022, p. 100089, from https://doi.org/10.1016/j.clce.2022.100089, 2023. DOI: 10.1016/j.clce.2022.100089

Ranz, W. E. and Marshall, W. R., Evaporation from Drops, *Chemical Engineering Progress*, 1952.

Rusche, H., Computational Dispersed Two-Phase Dynamics Flows of At Phase Fractions, no. 1, from http://hdl.handle.net/10044/1/8110, 2002.

Schiller, L. and Naumann, A. (1935) A Drag Coefficient Correlation. Zeitschrift des Vereins Deutscher Ingenieure, 77, 318-320.

Sutherland, W., The Viscosity of Gases and Molecular Force, *The London, Edinburgh, and Dublin Philosophical Magazine and Journal of Science*, vol. **36**, no. 223, pp. 507–31, 1893. DOI: 10.1080/14786449308620508

Wen, C. Y. and Yu, Y. H., A Generalized Method for Predicting the Minimum Fluidization Velocity, *AIChE Journal*, vol. **12**, no. 3, pp. 610–12, 1966. DOI: 10.1002/aic.690120343

7. RESPONSIBILITY NOTICE

The authors are the only responsible for the printed material included in this paper.